Available online at www.sciencedirect.com
ScienceDirect
Journal of the European Ceramic Society 29 (2009) 539–550
www.elsevier.com/locate/jeurceramsoc

Development of microstructure during creep of polycrystalline mullite and a nanocomposite mullite/5 vol.% SiC

S. Gustafsson [a], L.K.L. Falk [a,*], J.E. Pitchford [b], W.J. Clegg [b], E. Lidén [c], E. Carlström [c]

[a] *Department of Applied Physics, Chalmers University of Technology, SE-412 96 Göteborg, Sweden*
[b] *Department of Materials Science and Metallurgy, University of Cambridge, Pembroke Street, CB2 3QZ Cambridge, UK*
[c] *Swedish Ceramic Institute, Swerea IVF, Box 104, SE-431 22 Mölndal, Sweden*

Received 25 June 2008; accepted 27 June 2008
Available online 21 August 2008

Abstract

The microstructures of as-sintered and creep tested polycrystalline mullite and mullite reinforced with 5 vol.% nano-sized SiC particles have been characterized by scanning and transmission electron microscopy. The dislocation densities after tensile creep testing at 1300 and 1400 °C were virtually unchanged as compared to the as-sintered materials which indicates diffusion-controlled deformation. Mullite matrix grain boundaries bending around intergranular SiC particles suggest that grain boundary pinning, in addition to a reduced mullite grain size, contributed to the increased creep resistance of the mullite/5 vol.% SiC nanocomposite. Both materials showed pronounced cavitation at multi-grain junctions after creep testing at 1400 °C which suggests that unaccommodated grain boundary sliding, facilitated by softening of the intergranular glass, occurred at this temperature. This is consistent with the higher stress exponents at 1400 °C.

Keywords: Mullite; Nanocomposites; Grain boundaries; Electron microscopy; Creep

1. Introduction

The incorporation of nano-sized second-phase ceramic particles into a ceramic matrix may lead to significant improvements in the mechanical properties.[1–8] Ohji et al.[2] found that the creep rate of alumina reinforced with 17 vol.% SiC nanoparticles was three orders of magnitude lower, and the creep life 10 times longer, than that of single-phase alumina. Alumina reinforced with 5 vol.% SiC nanoparticles, studied by Thompson et al.,[3] showed an increase in creep resistance that was similar to Ohji's results, but the lower fraction of SiC particles resulted in a reduced number of intergranular creep cavities and a much longer creep life. As shown in several studies, a smaller volume fraction of nanoparticles, typically around 5 vol.%, is often sufficient in order to give a substantial improvement in the mechanical properties.[1,3,7,8]

The mechanism behind the pronounced improvements with smaller additions of a nano-sized second phase is, however, still not fully understood.[3,5,8] It has been suggested that the improved creep resistance of alumina/SiC nanocomposites is caused by the thermal mismatch between alumina and SiC.[5] Internal compressive stresses are introduced at the alumina/SiC interface, and this results in a stronger particle/matrix bonding and thereby an improved creep resistance.[5] It is, therefore, of interest to evaluate different matrix materials with different thermal expansion coefficients, and to characterize particle/matrix interface structures and properties.

Mullite, $3Al_2O_3{\cdot}2SiO_2$, is one potential matrix material in nanocomposite ceramics. Mullite has excellent high temperature properties, and its creep resistance is high compared to other oxide ceramics.[9–15] In the work by Lessing et al.[9] it was shown that the creep rate of polycrystalline mullite at 1450 °C was one order of magnitude lower than that of polycrystalline alumina of the same grain size. The thermal mismatch between mullite and SiC is, however, smaller than that between alumina and SiC.[16,17]

The present paper is focussed on the relationship between the fine-scale micro- and nanostructure and the creep deformation process in polycrystalline mullite and mullite reinforced with 5 vol.% nano-sized SiC particles. The microstructures

* Corresponding author. Tel.: +46 31 772 3321.
E-mail address: lklfalk@chalmers.se (L.K.L. Falk).

0955-2219/$ – see front matter © 2008 Elsevier Ltd. All rights reserved.
doi:10.1016/j.jeurceramsoc.2008.06.036

of as-fabricated and creep tested specimens were characterized by scanning and transmission electron microscopy (SEM, TEM), and particular attention was paid to the grain boundary regions and the location and size distribution of the SiC particles. The creep tests, and theoretical modelling for the prediction of the creep behaviour of these ceramics, have previously been carried out by Clegg and co-workers.[18,19] Results from that work, relevant to the electron microscopy investigation presented in this paper, are reviewed shortly below.

2. Review of creep test and modelling results

Polycrystalline mullite, and mullite reinforced with 5 vol.% SiC nanoparticles (in the following termed "the nanocomposite"), have been subjected to tensile creep tests in air at 1300 and 1400 °C under stresses between 10 and 50 MPa.[18,19] Theoretical modelling of diffusion-controlled creep deformation of these two materials was also carried out.[18,19]

2.1. Polycrystalline mullite

Creep tests of the polycrystalline mullite material at 1300 °C showed a stress exponent of $n = 1.2$ which implies that diffusion processes ($n = 1$) are controlling the creep deformation at this temperature, see Fig. 1a. Creep tests performed at 1400 °C resulted in a higher stress exponent of $n = 2$ (Fig. 1a), which suggests that, in addition to diffusion processes, other creep mechanisms become active at this temperature.

The experimentally determined creep rates were compared with creep rates expected for diffusion-controlled creep as given by

$$\dot{\varepsilon} = \frac{14\sigma\Omega}{kTd^2} D_{\text{eff}} \quad (1)$$

where σ is the applied stress, Ω the volume of the rate-controlling diffusing species, k the Boltzmann constant and d is the grain size. D_{eff} is the effective diffusion coefficient, related to the diffusion coefficients for lattice diffusion D_l and grain boundary diffusion D_b according to

$$D_{\text{eff}} = D_l + \frac{\pi\delta}{d} D_b \quad (2)$$

where δ is the grain boundary width. Maximum and minimum values of $D_{\text{eff}}\Omega$ at the two test temperatures were calculated from mullite creep data presented in the literature.[9,12,13,20] These values were then used in an estimate of the creep rate interval of the mullite ceramic in the present investigation ($d = 1.5$ μm).[18] The plots in Fig. 1a, based on data taken from Pitchford,[18] show that the experimentally determined creep rates at 1300 °C, and at higher stresses at 1400 °C, were higher than the predicted values.

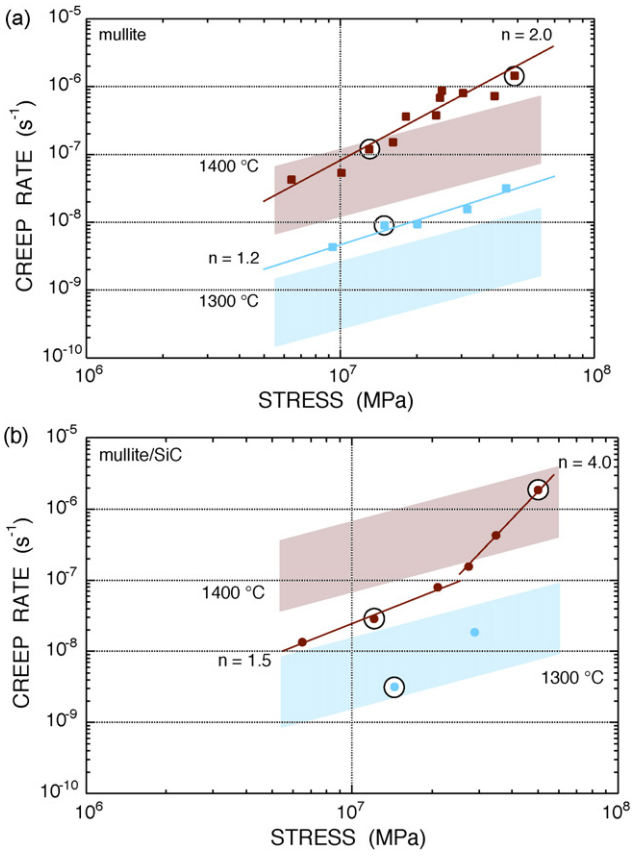

Fig. 1. Experimentally determined steady-state creep rates of (a) the polycrystalline mullite and (b) the mullite/5 vol.% SiC at 1300 and 1400 °C plotted as function of stress. The testing conditions for the specimens subjected to the microstructural characterization are marked by circles. Diffusional creep rate intervals of polycrystalline mullite, predicted for the grain sizes of the two experimental materials, are also shown plotted. Data taken from Pitchford[18].

2.2. Mullite reinforced with 5 vol.% SiC nanoparticles

The experimental creep rates of the nanocomposite at 1300 and 1400 °C are plotted in Fig. 1b. The creep tests at 1400 °C

Table 1
The as-sintered and creep tested materials

Material	Test temperature (°C)	Stress (MPa)	Steady-state creep rate (s^{-1})	Grain size (μm)
Polycrystalline mullite		As-sintered		1.5
	1400	48.6	1.5×10^{-6}	1.3
	1400	13.0	1.2×10^{-7}	1.5
	1300	14.9	9.5×10^{-9}	1.5
Mullite/SiC nanocomposite		As-sintered		0.7
	1400	50.0	1.9×10^{-6}	0.7
	1400	12.1	2.9×10^{-8}	0.8
	1300	14.4	3.2×10^{-9}	0.8

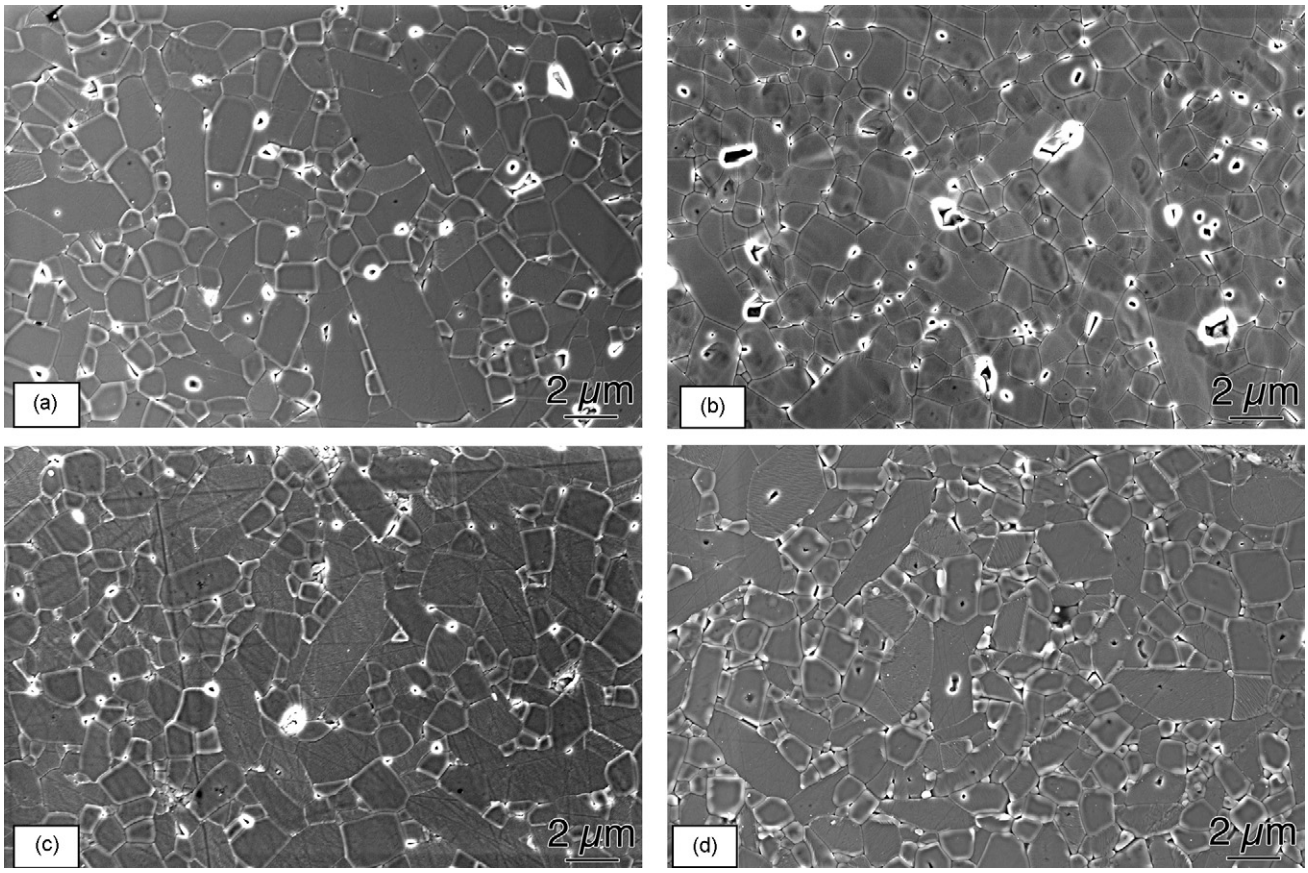

Fig. 2. Thermally etched surfaces of the polycrystalline mullite in the (a) as-sintered condition, and after creep testing under a stress of (b) 48.6 MPa at 1400 °C, (c) 13.0 MPa at 1400 °C, and (d) 14.9 MPa at 1300 °C.

showed that the stress exponent increased with increasing stress; from around $n = 1.5$ at stresses under 25 MPa to around $n = 4$ at stresses above 25 MPa. This implies that the total strain was not caused by one single creep mechanism.

The creep rate intervals for diffusion-controlled creep of polycrystalline mullite with a reduced average grain size ($d = 0.7$ μm, corresponding to the average matrix grain size of the nanocomposite) were calculated as described in Section 2.1.[18,19] This was done in order to better assess the effect of the SiC particles, and these creep rate intervals are also shown in Fig. 1b. As illustrated in Fig. 1b, the experimental creep rates of the nanocomposite tested at low stresses (<30 MPa) at 1400 °C were lower than the predicted diffusion creep rates of polycrystalline mullite with this grain size. At higher stresses, however, the creep rate of the nanocomposite was in the range predicted by the diffusion-controlled creep model. The two data points from creep tests at 1300 °C were within the predicted diffusion creep rate interval.

The data presented in Fig. 1b indicate that the creep rate of the nanocomposite was determined not only by the reduced mullite grain size. It has been suggested that the extra work required to drive self-diffusion in the low diffusivity SiC particles, so that they can move with the grain boundaries during creep, will lead to a reduced creep rate as compared to polycrystalline mullite of the same grain size.[19]

3. Experimental procedures

3.1. Materials

3.1.1. Polycrystalline mullite

The polycrystalline mullite material was produced by mixing commercially available 3:2 mullite powder (KM-101, Kyoritsu, Japan) and an ammonium polyacrylate dispersant (Dispex, Allied Colloids, England) in water. The slurry was ball milled for 24 h using zirconia ball milling beads. Green bodies were produced by slip casting and pressureless sintered in air at 1650 °C for 3 h. The material was 97% dense as measured by Archimedean densitometry.

3.1.2. Mullite/SiC nanocomposite

The α-SiC starting powder (UF-45, H.C. Starck, Germany) had a specific surface area of around 45 m^2/g. The larger particles and agglomerates that were difficult to break down by milling the powder were removed by sedimentation. This resulted in a milled and fractionated SiC starting powder that had a mean particle size (d_{50}) of 0.22 μm.

The nanocomposite material was then produced from an aqueous suspension containing 95 vol.% of the mullite powder, 5 vol.% of the milled and fractionated α-SiC powder, and 0.3 wt% of an ammonium polyacrylate dispersant (Duramax 3021, Rohm and Haas, Sweden). The suspension was

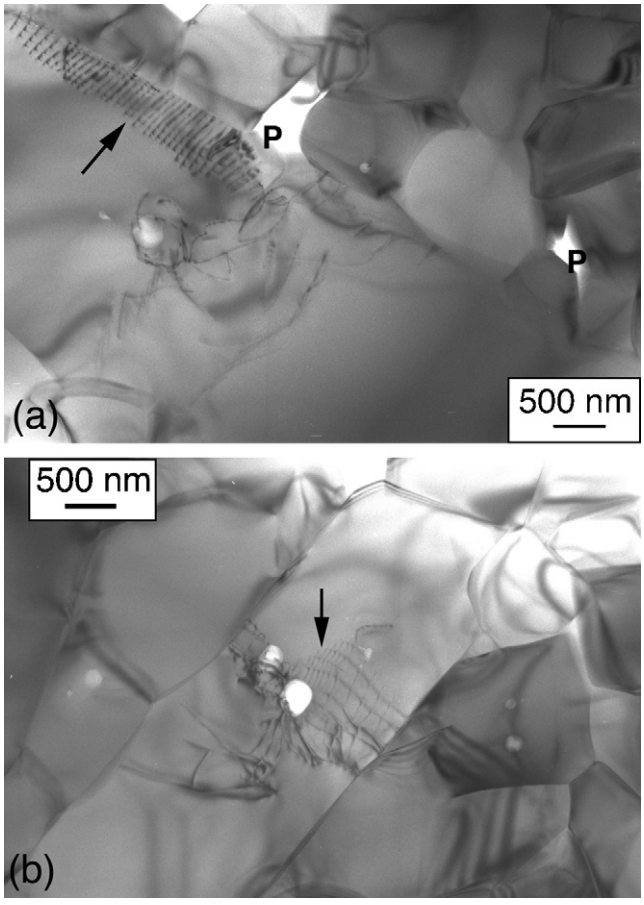

Fig. 3. The microstructure of the as-sintered polycrystalline mullite (TEM). (a) Intergranular porosity (P), and a dislocation pile-up at a grain boundary (arrowed). (b) Dislocation network (arrowed) associated with cavities on a larger elongated grain section.

homogenised by milling for 1 h in a planetary mill using Si_3N_4 balls whereafter 3 wt% of a polyethylene glycol binder was added to the slip. In order to retain a homogeneous distribution of the SiC nanoparticles, the slip was freeze granulated by spraying into liquid nitrogen. The ice was removed by sublimation using a freeze dryer and the resulting granules were hot pressed into plates at 1600 °C for 1 h in an argon atmosphere at a maximum pressure of 40 MPa. Hot pressing has been widely used for producing dense nanocomposite materials since the nanoparticles may suppress full densification.[2–4,6] The nanocomposite material in the present study reached nearly full density, 99.8%, as measured by a helium pycnometer.

3.2. Microstructural characterization and instrumentation

The as-sintered and creep tested materials included in the microstructural characterization are shown in Table 1. Polished and thermally etched (45 min at 1300 °C in argon) specimens were imaged in a SEM (Leo ULTRA 55) equipped with a field emission gun (FEG) in order to assess grain size and overall homogeneity. The average grain size was determined by the mean linear intercept method, and the average intercept length was multiplied by a factor of 1.5.

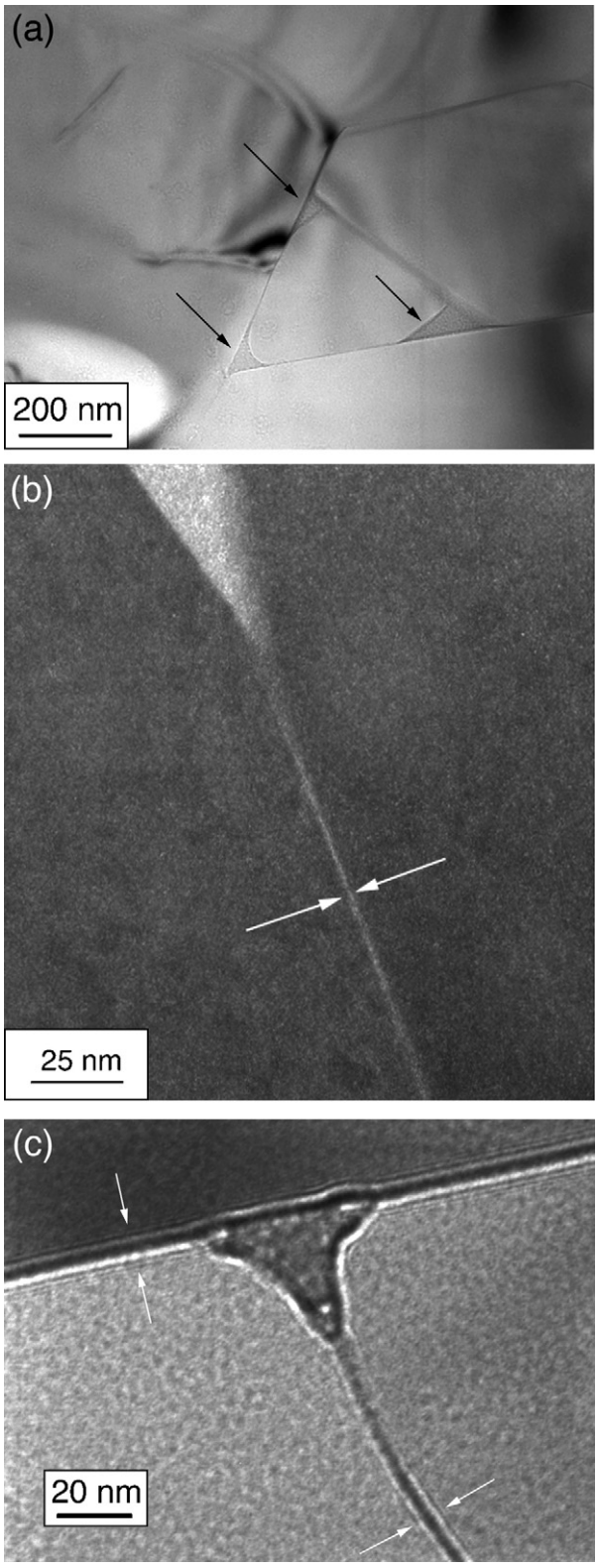

Fig. 4. Amorphous pockets at triple grain junctions and glassy grain boundary films in the as-sintered polycrystalline mullite (TEM). (a) Glass containing triple grain junctions (arrowed). (b) Diffuse dark field image of a thin glassy grain boundary film (arrowed) merging into an amorphous pocket. The glass appears with bright contrast. (c) Defocus Fresnel image of a triple grain junction. Fresnel fringes (arrowed) extending along the grain boundaries reveal the presence of thin intergranular films merging into a pocket at the triple grain junction.

Thin-foil specimens for TEM were prepared by standard specimen preparation techniques; mechanical grinding and polishing, dimpling and final ion milling to electron transparency. The microstructures were characterized in a Philips CM200 FEGTEM equipped with a Link ISIS energy dispersive X-ray (EDX) system and a Gatan Imaging Filter (GIF). The chemical composition of mullite grains and amorphous grain boundary regions was determined by fine probe EDX point analysis. Elemental profiles acquired by the EDX system attached to the FEGTEM were used for the evaluation of peak areas in the quantification of the EDX spectra. Due to the uncertainty in oxygen quantification, only the relative amounts of aluminum

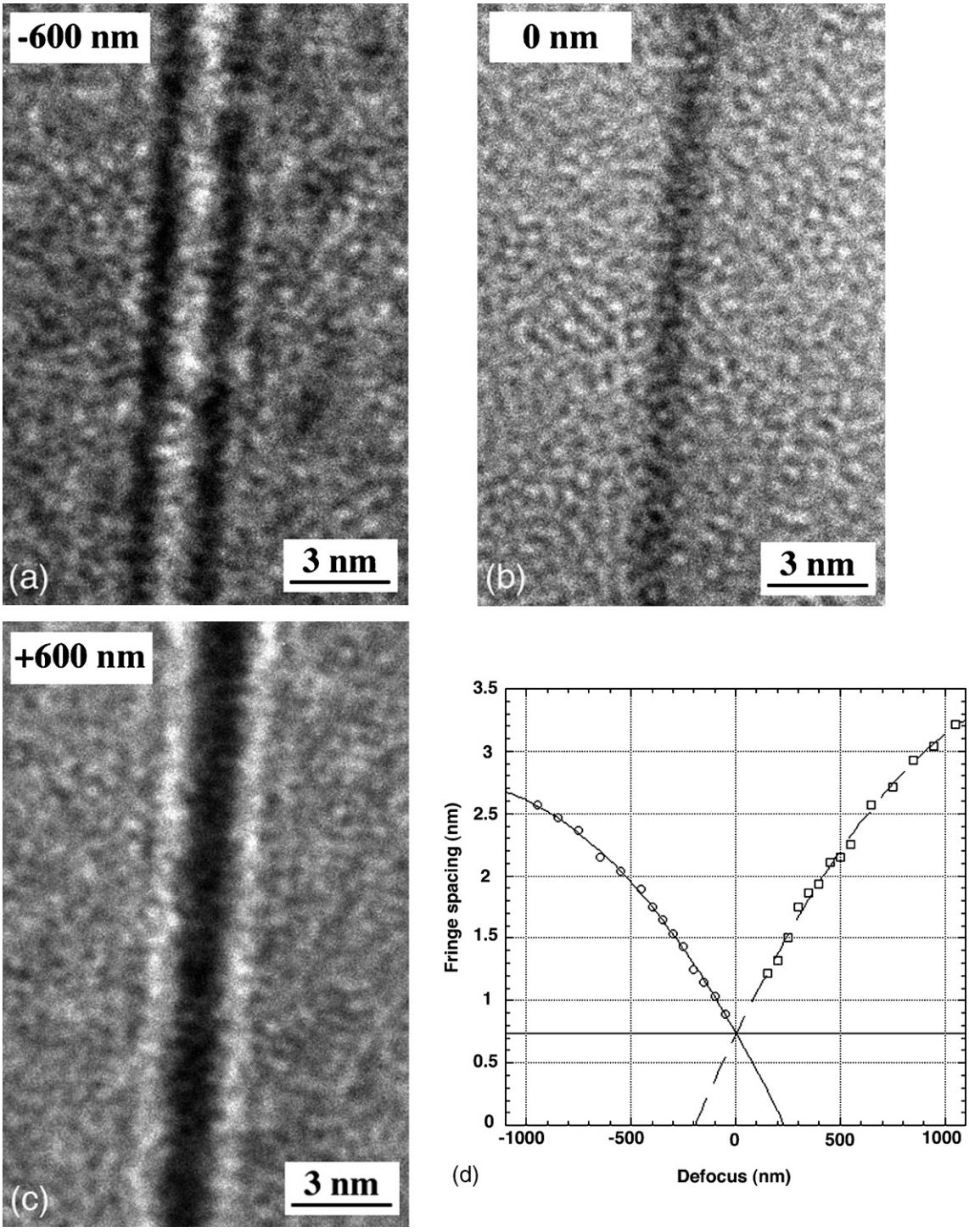

Fig. 5. Assessment of grain boundary film thickness in the as-sintered polycrystalline mullite using the defocus Fresnel imaging technique. (a) The underfocussed image shows a set of dark fringes parallel to the grain boundary. (b) At Gaussian focus there are no fringes. (c) The fringe contrast is reversed in the overfocussed image so that two bright lines delineate the boundary. (d) By plotting the fringe spacing as a function of defocus and extrapolating the data to Gaussian focus, it is possible to estimate the film thickness to, in this case, approximately 0.75 nm.

and silicon were determined. These were then converted into the equivalent mol fractions of alumina and silica.

Grain boundary films and amorphous regions were imaged in diffuse dark field, and the presence of grain boundary films was also established by defocus Fresnel imaging of edge-on grain boundaries.[21–25] The defocus Fresnel technique was used in estimating the thickness of the amorphous grain boundary film in around 20 randomly chosen grain boundaries in the as-sintered materials and in the mullite and nanocomposite specimens crept at 1400 °C under a stress of 48.6 and 50.0 MPa, respectively. The grain boundaries were oriented in the edge-on position by looking at the reflection symmetry of the fringe intensity across the boundary. Through-focus series were then recorded and processed with the Gatan DigitalMicrograph software. An intensity profile across a boundary was obtained by integrating the image over a distance of 10–15 nm along the boundary. The fringe separation was then determined from the intensity profiles and plotted as a function of defocus. The film thickness was estimated by extrapolating the data to Gaussian focus.

4. Results

4.1. The as-sintered polycrystalline mullite

The general microstructure of the as-sintered mullite material is shown in Figs. 2a and 3. Most grain sections were equiaxed, but a limited number of larger and elongated sections was also observed on the etched surfaces. The average grain size was determined to 1.5 μm. A smaller amount of residual porosity was observed throughout the microstructure, consistent with the density measurement (97% dense), see Fig. 3. Intergranular, irregularly shaped, cavities with sizes in the range 0.1–1 μm were present at some multi-grain junctions, while the grain boundaries were free of cavities.

Larger elongated grain sections often contained faceted intragranular cavities, 50–500 nm in size, but only a limited number of the equiaxed grain sections showed cavities. The intragranular cavities were often associated with single dislocations, or an odd dislocation network, as shown in Fig. 3b. The overall dislocation density in the microstructure was, however, low. Only occasional dislocation structures, such as pile-ups at grain boundaries (Fig. 3) and low angle grain boundaries, were observed.

Thin glassy grain boundary films merging into amorphous pockets at triple grain junctions were present throughout the microstructure, see Fig. 4. The amorphous triple grain junctions had a diameter (corresponding to the diameter of a circle of equivalent area) in the range 30–70 nm. All analysed amorphous grain boundary films were found to be in the range 0.6–0.9 nm thick. The result of a TEM through-focus series is shown in Fig. 5.

The mullite grains did not have a perfect 3:2 mullite composition; the mol fraction Al_2O_3 was 57.6 ± 2.0%, slightly lower

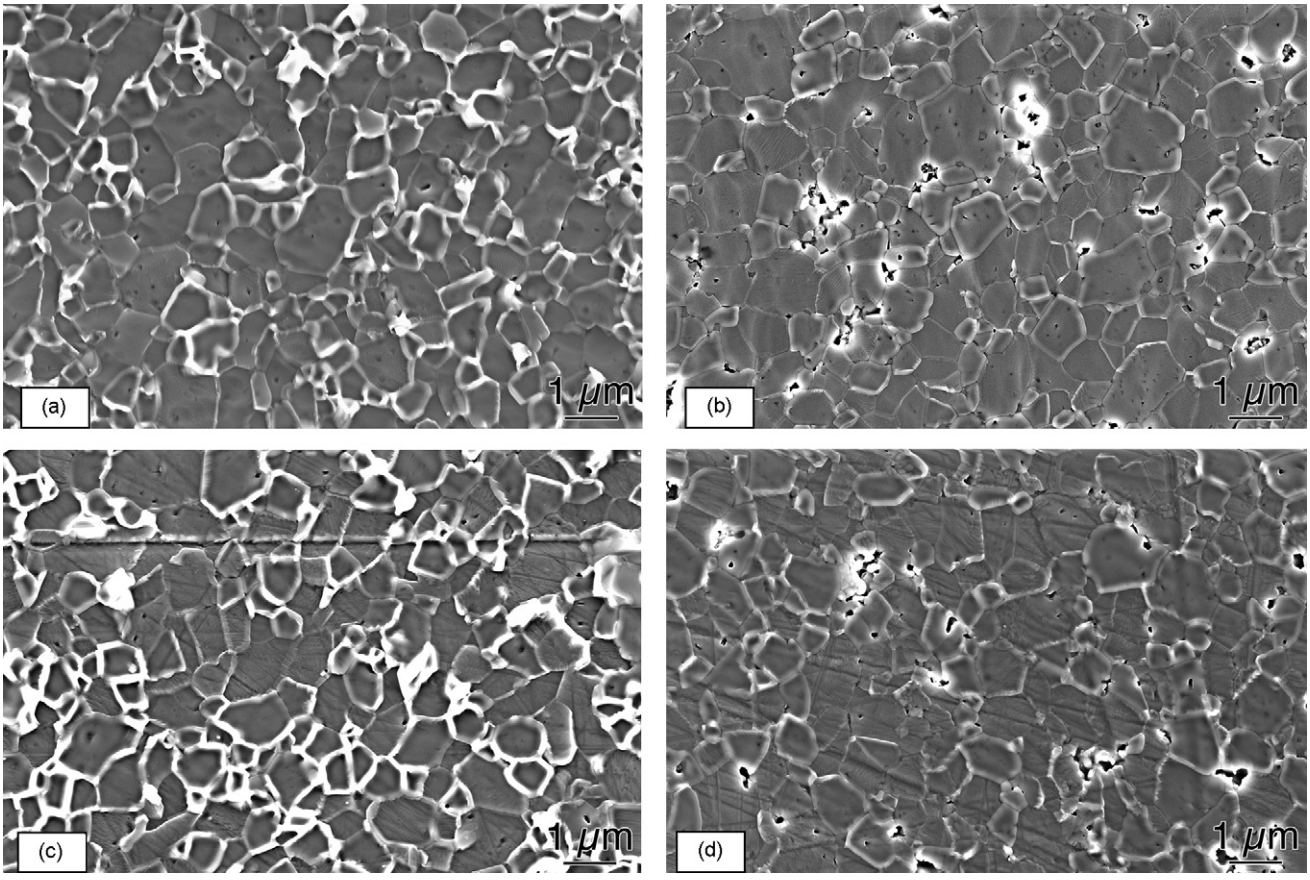

Fig. 6. Thermally etched surfaces of the nanocomposite in the (a) as-sintered condition, and after creep testing under a stress of (b) 50.0 MPa at 1400 °C, (c) 12.1 MPa at 1400 °C, and (d) 14.4 MPa at 1300 °C.

than the expected 60%. The glassy pockets at multi-grain junctions were rich in silicon. The mol fraction SiO_2 in the glass was $93.0 \pm 3.2\%$. Some of the analysed glassy pockets showed an alumina content close to the eutectic Al_2O_3–SiO_2 composition of approximately 5 mol% Al_2O_3, reported in several studies.[26,27] EDX also showed that the amorphous grain boundary films were rich in silicon. Impurities were not detected in any of these analyses.

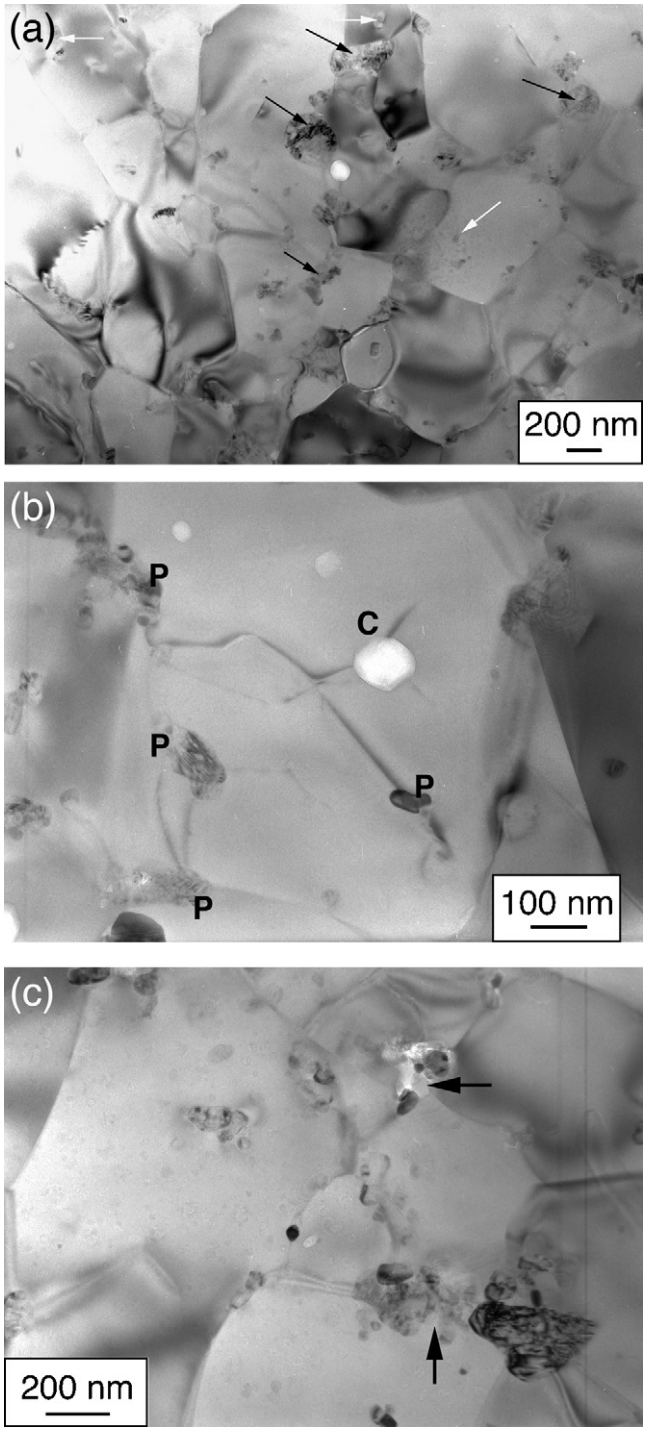

Fig. 7. The microstructure of the as-sintered nanocomposite (TEM). (a) SiC particles present in both inter- and intragranular positions (black and white arrows, respectively). (b) Dislocations pinned by intragranular cavities (C) and SiC particles (P). (c) Clusters of SiC particles (arrowed), associated with intergranular porosity.

4.2. The as-sintered mullite/SiC nanocomposite

The microstructure of the as-sintered nanocomposite material is shown in Figs. 6a and 7. Most grain sections were equiaxed, and an average matrix grain size of 0.7 μm was determined from SEM images (Figs. 6 and 7a). The mullite grains contained intragranular cavities also in this microstructure, and these cavities were usually faceted and less than 100 nm in diameter (Fig. 7b).

The majority (around 80%) of the SiC particles were located at grain boundaries and multi-grain junctions, see Fig. 7. The size of these particles was in the range 30–90 nm, and a number of them formed agglomerates as shown in Fig. 7. Particle agglomerates present in multi-grain junctions were generally associated with cavities, see Fig. 7c. The intragranular SiC particles did not form clusters, and were smaller, typically 10–50 nm, see Fig. 7a. Strain contours were only occasionally observed in the mullite matrix immediately surrounding a SiC particle.

Some dislocations were pinned by, or emerging from, the intra- and intergranular SiC particles, but the majority of the observed dislocations were, as in the mullite microstructure, associated with intragranular cavities, see Fig. 7b. Although the overall dislocation density was low, dislocation pile-ups at triple grain junctions or at grain boundaries were observed in a few areas.

Thin glassy films were observed in the matrix grain boundaries along with smaller volumes of glass separating both intragranular and intergranular SiC particles from the surrounding mullite grains, see Figs. 8 and 9. The thickness of the amorphous grain boundary films varied between 0.6 and 0.9 nm. Very small (~10–15 nm) amorphous pockets were observed at some multi-grain junctions, see Fig. 8.

The Al_2O_3 mol fraction of the mullite matrix was determined to $55.9 \pm 1.5\%$, i.e. also in this case lower than for 3:2 mullite. The intergranular glass was enriched in silicon, although the

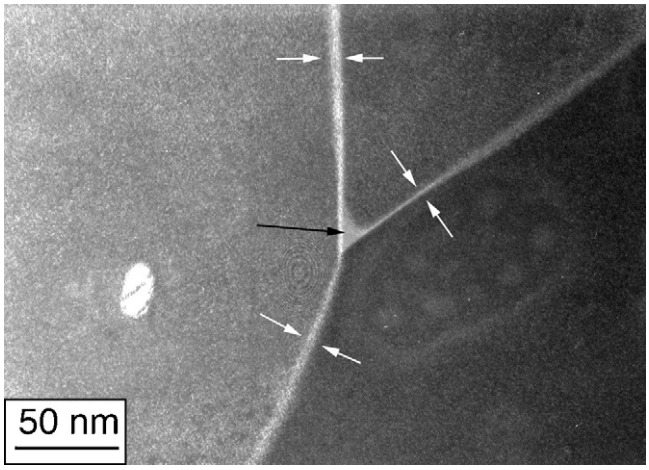

Fig. 8. Thin glassy grain boundary films (white arrows) merging into a glass containing triple grain junction (black arrow) in the as-sintered nanocomposite material. The glass appears with bright contrast in the diffuse TEM dark field image.

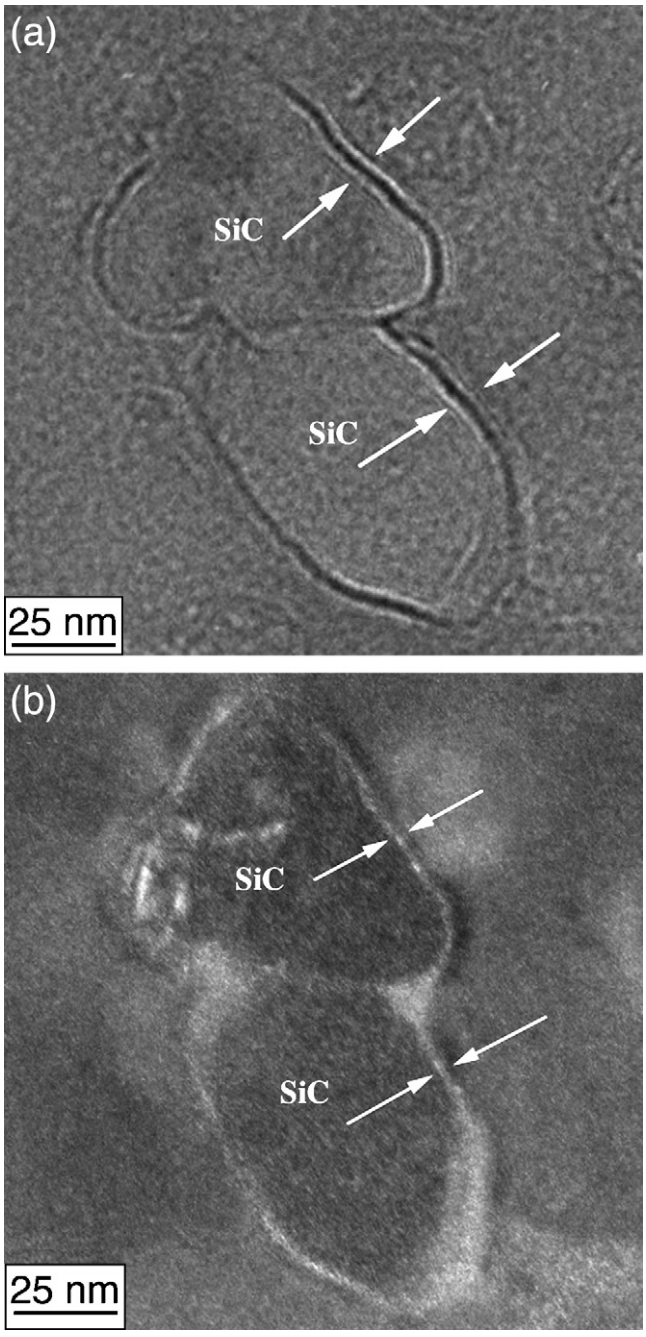

Fig. 9. Thin amorphous films separating intragranular SiC particles from the surrounding mullite grain in the as-sintered nanocomposite. (a) Defocus Fresnel fringes (arrowed). (b) Diffuse dark field image. The glassy films (arrowed) appear with bright contrast.

glass volumes in the thin-foil TEM specimens were too small for quantitative analysis.

4.3. The polycrystalline mullite after creep testing

The average grain sizes of the creep tested mullite specimens were virtually the same as that of the as-sintered material, see Table 1. This indicates that grain growth was not significant during creep testing, see Fig. 2.

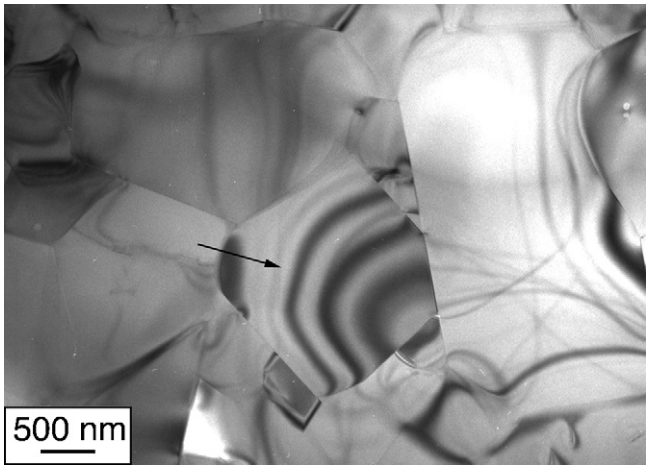

Fig. 10. A grain showing strain contours (arrowed) in the TEM thin-foil specimen of the polycrystalline mullite crept under a stress of 13.0 MPa at 1400 °C.

Strain contours were generally observed in the TEM bright field images of the microstructures of the crept mullite specimens as shown in Figs. 10 and 11. These contours reflect the stresses that built up in the material during creep deformation.

An increased cavitation at multi-grain junctions was observed in some areas of the crept microstructures, see Fig. 11. This type of cavitation was most pronounced in the specimen that had been subjected to the highest stress (48.6 MPa) at 1400 °C, but also evident in the specimen crept under a stress of 14.9 MPa at 1300 °C. The microstructure of the specimen crept under a stress of 13.0 MPa at 1400 °C resembled, on the other hand, that of the as-sintered material, with only a limited increase in the density of cavities.

A number of the intragranular cavities changed shape or size during creep testing, and in some cases thin channels connecting nearby cavities had developed, see Fig. 12. The size of these cavities ranged from several hundred nanometers up to 1 μm.

The overall dislocation density was low also in the creep tested mullite specimens. Dislocations were present

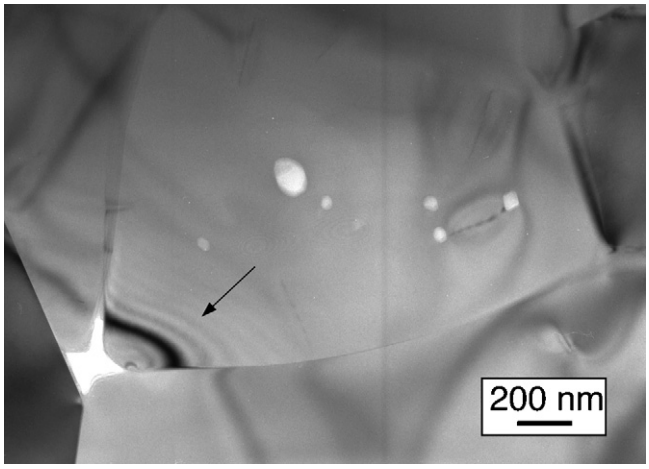

Fig. 11. Cavity formation in a multi-grain junction in the polycrystalline mullite creep tested under a stress of 48.6 MPa at 1400 °C. One of the grains shows strain contours (arrowed).

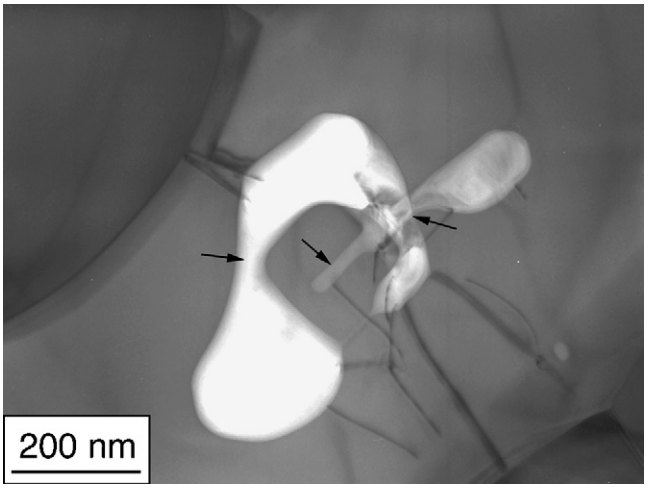

Fig. 12. Intragranular cavities in the polycrystalline mullite crept under a stress of 14.9 MPa at 1300 °C. Thin channels (arrowed) are connecting, or extending out from, the enlarged cavities.

predominantly in the larger grain sections, and in general associated with intragranular cavities, as in the as-sintered material.

Glass pockets at multi-grain junctions and thin amorphous grain boundary films were present also in the crept microstructures. Measurements of the film thickness in the sample crept at 1400 °C under a stress of 48.6 MPa did not reveal any pronounced changes in the thickness as compared to the as-sintered mullite material; the films had a thickness of, typically, 0.6–0.9 nm also after creep testing.

4.4. The nanocomposite after creep testing

Grain size measurements on the creep tested mullite nanocomposite specimens did not show any evidence of grain growth during creep deformation, see Table 1 and Fig. 6. The location and distribution of the SiC particles was also apparently unchanged, see Fig. 13. Around 80% of the SiC particles were located at the grain boundaries and multi-grain junctions in the specimen that had been crept at 1400 °C under a stress of 50.0 MPa. The mullite/mullite grain boundaries were often observed to bend near the intergranular SiC particles, see Fig. 14.

An increased number of the multi-grain junctions, predominantly junctions containing intergranular SiC particles, contained cavities after creep testing. This was particularly pronounced in the specimen crept under the highest stress, 50 MPa, at 1400 °C, see Fig. 13b. Cavitation associated with the SiC particles at the grain boundaries was rarely observed. The cavities inside the mullite matrix grains seemed to have retained their size and shape during creep testing.

The dislocation densities in the creep tested nanocomposite specimens were low and seemingly unchanged as compared to the as-sintered material. A limited number of grains with a locally increased dislocation density were observed in the crept microstructures, but these areas were not different from similar areas in the as-sintered nanocomposite microstructure.

Thin intergranular glassy films were present also after creep testing. Measurements of the grain boundary film thickness in the sample crept at 1400 °C under a stress of 50 MPa, showed

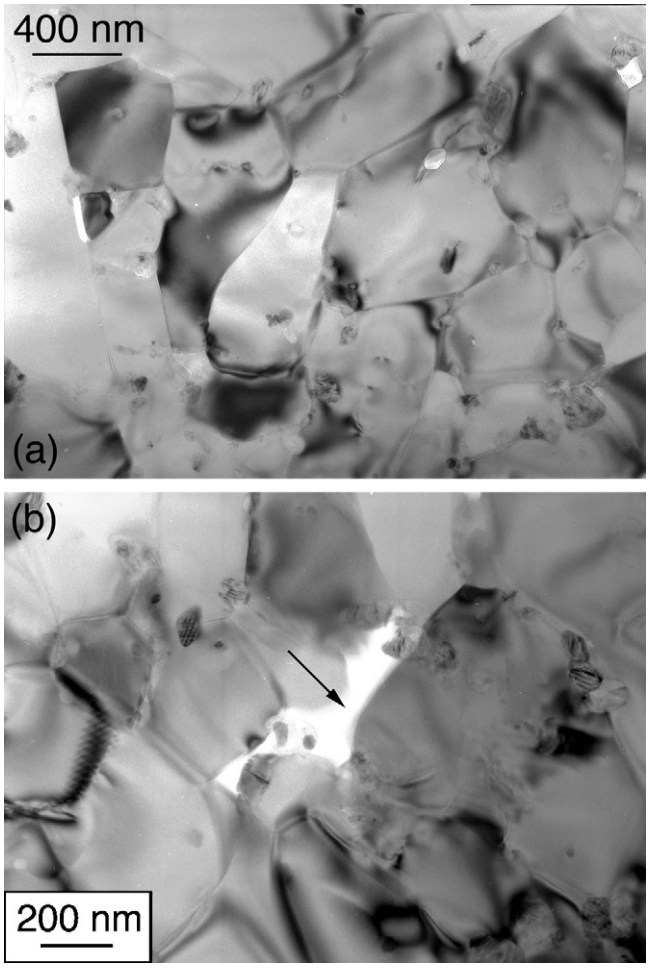

Fig. 13. The general microstructure (a) and cavity formation (arrowed) at multi-grain junctions (b) of the nanocomposite after creep testing under a stress of 50.0 MPa at 1400 °C.

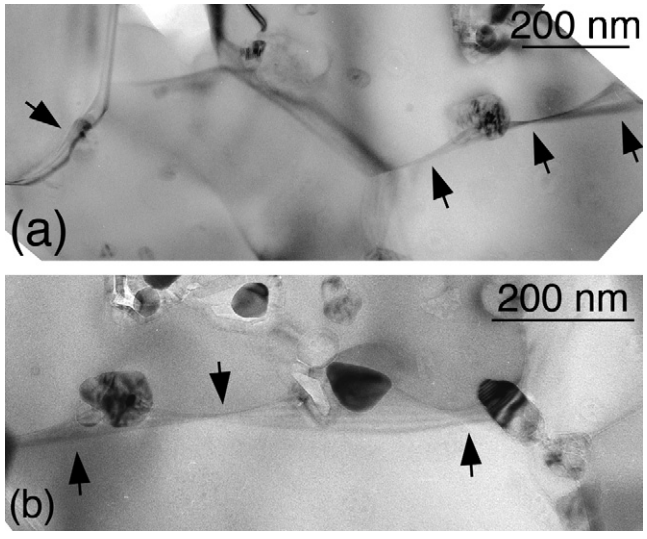

Fig. 14. Mullite matrix grain boundaries bending (arrowed) around intergranular SiC particles after creep testing under a stress of 50.0 MPa at 1400 °C.

film widths in the range 0.6–0.9 nm. The creep deformation process, did, hence, not have any pronounced effect on the distribution of the intergranular glass.

5. Discussion

5.1. The polycrystalline mullite

The virtually unchanged low dislocation densities in the crept mullite specimens strongly suggest that dislocation glide was not active to any significant extent under the applied testing conditions. This is in agreement with previous experimental studies which indicated a very limited (if any at all) dislocation mobility during plastic deformation of both single crystal and polycrystalline mullite specimens.[10,12,13,28] A previous TEM investigation of dislocations in mullite by Gustafsson and Falk[29,30] revealed comparatively large Burgers vectors of the type **b** = <1 0 0>, <0 1 0>, <1 1 0> and <1 1 2>. This may, together with the complex mullite crystal structure, result in a limited dislocation activity.[12]

The changes observed in the microstructures of the crept mullite specimens indicate that lattice diffusion is an active creep deformation mechanism, both at 1300 and 1400 °C. The elongation and enlargement of some intragranular cavities, and the development of thin intragranular cavity channels, indicate diffusion activity within the grains, and thus a contribution from Nabarro-Herring creep. In addition, the presence of a continuous intergranular glassy phase at the grain boundaries (Figs. 4 and 5) would provide rapid diffusion paths and thereby promote creep deformation by grain boundary diffusion. The intergranular glass may, hence, contribute to an increased creep rate as compared to the model discussed in Section 2, see Fig. 1a.

Creep deformation by diffusion, either through the grains or through the grain boundary glass, would give a stress exponent of $n = 1$. This is in good agreement with the stress exponent of $n = 1.2$ that was determined from the creep tests performed at 1300 °C.[18] Solution-reprecipitation creep, limited by the transport of matter through the glassy grain boundary films, is also expected to give a stress exponent of $n = 1$. There is, however, no microstructural evidence for such a process.

Diffusion creep only would, however, not result in the stress exponent $n = 2$ determined from the creep tests carried out at 1400 °C.[18] A large number of cavities had formed at multi-grain junctions in these specimens (Fig. 11), and the surrounding grains showed strain contrast (Figs. 10 and 11). This was most pronounced in the specimen that had been tested at 48.6 MPa. These observations suggest that rigid grain boundary sliding, facilitated by softening of the intergranular glass, contributed to the strain during creep testing. Such a process would increase the stress exponent, since cavitation alone gives values of $n > 1$.[31] A stress exponent close to $n = 2$, and evidence of cavitation and grain boundary sliding, have been observed previously in other creep studies of glass containing mullite ceramics.[10,12,13]

It may be expected that the amorphous grain boundary phase would redistribute during rigid grain sliding because the glass may be squeezed out from grain boundaries under compression and accumulated in grain boundaries under tension.[32] The measurements of intergranular film widths presented in this paper do not, however, show any clear evidence of glass redistribution during these creep tests. The thickness of the investigated grain boundary films was in the range 0.6–0.9 nm in both as-sintered and crept specimens, and a possible redistribution might, therefore, be difficult to detect.

5.2. The mullite/SiC nanocomposite

The addition of SiC nanoparticles resulted in a reduced mullite grain size (Table 1). This indicates that the nanoparticles suppressed grain growth during sintering through grain boundary pinning. The SiC particles located at the grain boundaries were larger (30–90 nm) than the intragranular particles (10–50 nm). A critical SiC particle size for effective mullite grain boundary pinning would, hence, be in the range 30–50 nm during hot pressing under a pressure of 40 MPa at 1600 °C.

Strain contours were generally not observed in the mullite matrix around the SiC particles in the as-sintered specimen. This indicates that the thermal expansion mismatch between mullite ($\alpha = 5.3 \times 10^{-6}\,°C^{-1}$)[16] and SiC ($\alpha = 4.7 \times 10^{-6}\,°C^{-1}$)[17] is too low for the introduction of compressive residual stresses of any significant magnitude at the SiC/mullite interface. In addition, the analysed SiC/mullite interfaces contained amorphous films or pockets (Fig. 9). The SiC/mullite interfaces are, hence, not likely to be significantly more rigid than the glass containing mullite/mullite grain boundaries. This is in contrast to SiC reinforced alumina nanocomposites where the thermal expansion mismatch between alumina ($\alpha = 8.8 \times 10^{-6}\,°C^{-1}$)[17] and SiC puts the particle/matrix interface under compression during cooling from the sintering temperature. It has been proposed that this leads to a more rigid interface bonding and thereby to a reduced creep rate due to the suppression of the nucleation and annihilation of point defects during creep deformation.[5] The proposed rigid interface bonding was supported by theoretical calculations and TEM observations of glass free SiC/alumina interfaces.[5] This interface mechanism would, hence, not be active to any significant extent in the present mullite/SiC nanocomposite material.

The fraction of SiC particles located at mullite grain boundaries and multi-grain junctions was unchanged (80%) in the specimen that had been creep tested under a stress of 50.0 MPa at 1400 °C. This suggests that moving grain boundaries dragged the SiC particles during creep deformation. This process requires a directional flow of atoms from one side of the particle to the other.[33] The diffusional migration may occur along three different paths: through the SiC particle, in the thin glassy film separating the SiC particle from the mullite matrix or around the particle through the matrix. One of these diffusion processes, or interfacial reactions, may be rate controlling.[33]

A model proposed by Clegg and co-workers[18,19] suggests that the creep rate would be limited by self-diffusion through the low diffusivity SiC particles. It was assumed that the particles would move with a velocity equal to that of the grain boundary at which they are situated. It was also assumed that the global deformation of the body would be caused by self-diffusion within

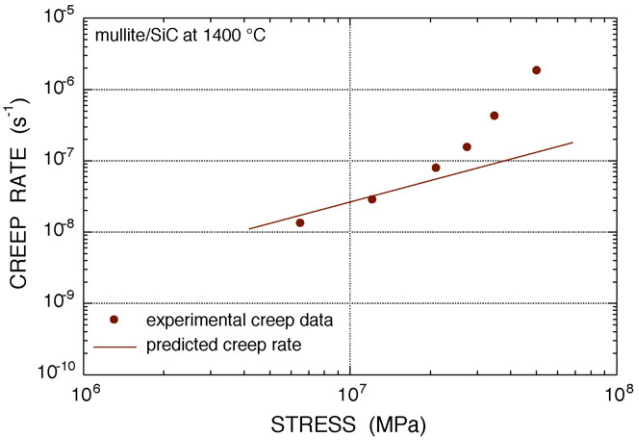

Fig. 15. The predicted nanocomposite creep rate at 1400 °C based on the assumption that SiC self-diffusion is rate limiting.[18,19] The experimentally determined steady-state creep rates of the nanocomposite at 1400 °C are also shown. Data taken from Pitchford[18].

the mullite matrix and within the SiC particles, and that these two processes would operate independently. The nanocomposite creep rates predicted at 1400 °C under these assumptions are shown in Fig. 15 together with the experimentally determined creep rates at this temperature. There is a relatively good agreement between the predicted and experimental creep rates at low stresses (<25 MPa), which indicates that creep under those conditions may be controlled by self-diffusion through the SiC particles. This is also suggested by the observation of SiC particle pinning of mullite/mullite grain boundaries (Fig. 14). The TEM investigation revealed, however, that there is usually a thin glassy film separating a SiC particle from the mullite matrix. This glass would not only provide a more efficient diffusion path, but also be a viscous medium facilitating rigid particle/matrix movement.[34]

The nanocomposite specimen crept under a stress of 50.0 MPa at 1400 °C showed a significantly increased cavitation at the multi-grain junctions. This suggests that unaccommodated grain boundary sliding, facilitated by a reduced viscosity of the grain boundary glass, had taken place. These observations may explain the increased stress exponent at higher stresses at 1400 °C and the discrepancy between the proposed model and the experimental creep data at these stresses (Figs. 1 and 15).

The TEM results indicated that the dislocation activity was very limited also during creep of the mullite/SiC nanocomposite material. The low dislocation density was virtually unchanged in the creep tested specimens. The combined results, hence, point towards diffusion-controlled creep processes at lower stresses and a transition to creep controlled by diffusion and rigid grain boundary sliding under higher stresses at 1400 °C.

6. Concluding remarks

Creep of polycrystalline mullite at 1300 °C is controlled by diffusion, but the smaller volumes of grain boundary glass increases the creep rate as compared to a pure mullite ceramic. At 1400 °C, grain boundary sliding, facilitated by softening of the intergranular glass, dominates the creep behaviour as suggested by the TEM observation of cavitation at multi-grain junctions and the presence of strain contours in adjacent mullite grains. This is consistent with the increase in the stress exponent from $n = 1.2$ at 1300 °C to $n = 2$ at 1400 °C.

The mullite/5 vol.% SiC nanocomposite has an increased creep resistance which is caused by grain boundary pinning by intergranular SiC particles and a reduced matrix grain size. Creep at 1300 °C, and at lower stresses at 1400 °C, is dominated by diffusion, and may be controlled by the slower self-diffusion in the SiC particles as compared to the mullite matrix. Multi-grain junction cavitation under higher stresses at 1400 °C, caused by rigid grain boundary sliding facilitated by softening of an intergranular amorphous phase, reduces the positive effect of the SiC nanoparticles. This results in a stress exponent that increases with stress at 1400 °C.

Acknowledgement

Financial support from the Swedish Foundation for Strategic Research and from AIST, NEDO, Japan through the Synergy Ceramics project is gratefully acknowledged.

References

1. Niihara, K., New design concept of structural ceramics—ceramic nanocomposites. *J. Ceram. Soc. Jpn.*, 1991, **99**(10), 974–982.
2. Ohji, T., Nakahira, A., Hirano, T. and Niihara, K., Tensile creep behaviour of alumina/silicon carbide nanocomposite. *J. Am. Ceram. Soc.*, 1994, **77**(12), 3259–3562.
3. Thompson, A. M., Chan, H. M. and Harmer, M. P., Tensile creep of alumina/silicon carbide nanocomposite. *J. Am. Ceram. Soc.*, 1997, **80**(9), 221–228.
4. Winn, A. J. and Todd, R. I., Microstructural requirements for alumina–SiC nanocomposites. *Br. Ceram. Trans.*, 1999, **98**(5), 219–224.
5. Ohji, T., Hirano, T., Nakahira, A. and Niihara, K., Particle/matrix interface and its role in creep inhibition in alumina/silicon carbide nanocomposites. *J. Am. Ceram. Soc.*, 1996, **79**(1), 33–45.
6. Stearns, L. C., Zhao, J. and Harmer, M. P., Processing and microstructure development in Al_2O_3–SiC nanocomposites. *J. Eur. Ceram. Soc.*, 1992, **10**, 473–477.
7. Ohji, T., Jeong, Y.-K., Choa, Y.-H. and Niihara, K., Strengthening and toughening mechanisms of ceramic nanocomposites. *J. Am. Ceram. Soc.*, 1998, **81**(6), 1453–1460.
8. Sternitzke, M., Review: structural ceramic nanocomposites. *J. Eur. Ceram. Soc.*, 1997, **17**, 1061–1082.
9. Lessing, P. A., Gordon, R. S. and Mazdiyasni, K. S., Creep of polycrystalline mullite. *J. Am. Ceram. Soc.*, 1975, **58**, 149.
10. Okamoto, Y., Fukudome, H., Hayashi, K. and Nishikawa, T., Creep deformation of polycrystalline mullite. *J. Eur. Ceram. Soc.*, 1990, **6**, 161–168.
11. Descamps, P., Poortemann, M. and Cambier, F., Thermomechanical properties and creep of mullite from rapidly quenched powders. *Key Eng. Mater.*, 1997, **132–136**, 595–598.
12. Dokko, P. C., Pask, J. A. and Mazdyasni, K. S., High-temperature mechanical properties of mullite under compression. *J. Am. Ceram. Soc.*, 1977, **60**(3–4), 150–155.
13. Hynes, A. P. and Doremus, R. H., High-temperature compressive creep of polycrystalline mullite. *J. Am. Ceram. Soc.*, 1991, **74**(10), 2469–2475.
14. Calderon-Moreno, J. M. and Torrecillas, R., High-temperature creep of polycrystalline mullite. *Key Eng. Mater.*, 1997, **132–136**, 587–590.
15. Schneider, H., Okada, K. and Pask, J. A., *Mullite and Mullite Ceramics*. John Wiley & Sons, Chichester, UK, 1994.
16. Kingery, W. E., Bowen, H. K. and Uhlmann, D. R., *Introduction to Ceramics* (*second edition*). John Wiley & Sons, US, 1976, p. 595.

17. Touloukian, Y. S., Kirby, R. K., Taylor, R. E. and Lee, T. Y. R. ed., *Thermophysical Properties of Matter*, *vol. 13*. Plenum Press, New York, 1985.
18. Pitchford, J. E., *Effects of Structure on Mechanisms and High Temperature Plastic Deformation in Oxide Ceramics*. PhD thesis. University of Cambridge, UK, 1999.
19. Pitchford, J. E., Lidén, E., Gustafsson, S., Falk, L. K. L., Carlström, E. and Clegg, W. J., The effect of particle migration on the creep-rate of nanocomposites. *Key Eng. Mater.*, 2006, **317–318**, 445–448.
20. Nixon, R. D., Chevacharoenkul, S., Davis, R. F. and Tiegs, T. N., Creep of hot-pressed SiC whisker reinforced mullite. *Ceram. Trans.*, 1990, **6**, 579–603.
21. Clarke, D. R., On the detection of thin intergranular films by electron microscopy. *Ultramicroscopy*, 1979, **4**, 33–44.
22. Ness, J. N., Stobbs, W. M. and Page, T. F., A TEM Fresnel diffraction based method for characterizing thin grain boundary and interfacial films. *Phil. Mag. A*, 1986, **54**(5), 679–702.
23. Cinibulk, M. K., Kleebe, H.-J. and Rühle, M., Quantitative comparison of TEM techniques of determining amorphous intergranular film thickness. *J. Am. Ceram. Soc.*, 1993, **76**(2), 426–432.
24. Falk, L. K. L., Electron spectroscopic imaging and fine probe EDX analysis of liquid phase sintered ceramics. *J. Eur. Ceram. Soc.*, 1998, **18**, 2263–2279.
25. Krivanek, O. L., Shaw, T. M. and Thomas, G., Imaging of thin intergranular phases by high resolution electron microscopy. *J. Appl. Phys.*, 1979, **50**(6), 4223–4227.
26. Aramaki, S. and Roy, R., Revised phase diagram for the system Al_2O_3–SiO_2. *J. Am. Ceram. Soc.*, 1962, **45**(5), 229–242.
27. Aksay, I. A. and Pask, J. A., Stable and metastable equilibria in the system SiO_2–Al_2O_3. *J. Am. Ceram. Soc.*, 1975, **58**(11–12), 507–512.
28. Aksay, I. A., Dabbs, D. M. and Sarikaya, M., Mullite for structural, electronic and optical applications. *J. Am. Ceram. Soc.*, 1991, **74**, 2343–2358.
29. Gustafsson, S. and Falk, L. K. L., Investigation of dislocations in mullite using LACBED. In *Proceedings of the 15th International Congress on Electron Microscopy (ICEM-15)*, 2002, pp. 1027–1028.
30. Gustafsson, S. and Falk, L. K. L., Defocus convergent beam electron diffraction analysis of dislocations in mullite. *J. Microsc.*, under review.
31. Luecke, W. E., Wiederhorn, S. M., Hockey, B. J., Krause Jr., R. F. and Long, G. G., Cavitation contributes substantially to tensile creep in silicon nitride. *J. Am. Ceram. Soc.*, 1995, **78**(8), 2085–2096.
32. Jin, Q., Wilkinson, D. S., Weatherly, G. C., Luecke, W. E. and Wiederhorn, S. M., Thickness alteration of grain-boundary amorphous films during creep of a multiphase silicon nitride ceramic. *J. Am. Ceram. Soc.*, 2001, **84**(6), 1296–1300.
33. Gleiter, H., Microstructure. In *Physical Metallurgy*, ed. R. W. Cahn and P. Haasen. fourth revised and enhanced edition Elsevier Science B.V., Amsterdam, 1996, pp. 887–889.
34. Luecke, W. E. and Wiederhorn, S. M., A new model for tensile creep of silicon nitride. *J. Am. Ceram. Soc.*, 1999, **82**(10), 2769–2778.